ORNL/TM-2024/3244
CRADA/NFE-20-08161

High Strength Aluminum Additive Manufacturing

Alex Plotkowski
Ryan Dehoff
Russ Cochran

October 1, 2023

OAK RIDGE NATIONAL LABORATORY
MANAGED BY UT-BATTELLE FOR THE US DEPARTMENT OF ENERGY

ORNL/TM-2024/3244
CRADA/ NFE-20-08161

Materials Science and Technology Division
Advanced Manufacturing Office

High Strength Aluminum Additive Manufacturing

Alex Plotkowski
Ryan Dehoff
Russ Cochran

Date Published:
October 1, 2023

Prepared by
OAK RIDGE NATIONAL LABORATORY
Oak Ridge, Tennessee 37831-6283
managed by
UT-BATTELLE, LLC
for the
US DEPARTMENT OF ENERGY
under contract DE-AC05-00OR22725

CONTENTS

LIST OF FIGURES

ACKNOWLEDGEMENTS

This CRADA NFE-20-08161was conducted as a Technical Collaboration project within the Oak Ridge National Laboratory (ORNL) Manufacturing Demonstration Facility (MDF) sponsored by the US Department of Energy Advanced Manufacturing Office (CPS Agreement Number 24761). Opportunities for MDF technical collaborations are listed in the announcement "Manufacturing Demonstration Facility Technology Collaborations for US Manufacturers in Advanced Manufacturing and Materials Technologies" posted at http://web.ornl.gov/sci/manufacturing/docs/FBO-ORNL-MDF-2013-2.pdf. The goal of technical collaborations is to engage industry partners to participate in short-term, collaborative projects within the Manufacturing Demonstration Facility (MDF) to assess applicability and of new energy efficient manufacturing technologies. Research sponsored by the U.S. Department of Energy, Office of Energy Efficiency and Renewable Energy, Advanced Manufacturing Office, under contract DE-AC05-00OR22725 with UT-Battelle, LLC.

ABSTRACT

High-strength aluminum alloys for elevated temperature applications are desirable to replace heavier and more expensive titanium alloys. However, most aluminum alloys lose a large fraction of their strength at temperatures above approximately 200°C. ORNL has designed DuAlumin-3D, an alloy with nominal composition Al-9Ce-4Ni-0.5Mn-1Zr (wt.%), which utilizes the high cooling rates in additive manufacturing (AM) to achieve a refined microstructure, and thermally stable mechanical properties. DuAlumin-3D was fabricated by laser powder bed fusion and tested for its tensile mechanical properties across a range of temperature, and for its room temperature high-cycle fatigue resistance. The alloy was tested in both the as-printed and heat treated conditions, and both parallel and perpendicular to the AM build direction. The alloy was found to have anisotropic mechanical behavior in the as-printed state, but the anisotropy significantly decreased (both for tensile and fatigue properties) following heat treatment. The tensile properties significantly out-performed benchmark wrought 2219-T61 across a wide temperature range. The room temperature fatigue performance was approximately similar to 2219-T61.

1. HIGH STRENGTH ALUMINUM ADDITIVE MANUFACTURING

This phase 1 technical collaboration project (MDF-TC-2020-185) was begun on April 1, 2020 and was completed on October 1, 2022. The purpose of this study was to perform an initial evaluation of DuAlumin-3D, an ORNL designed high-temperature Al alloy for additive manufacturing, for application to aerospace components.

1.1 BACKGROUND

The performance and efficiency of aerospace systems may be significantly improved through reductions in weight. Additive manufacturing (AM) of light-weight aluminum alloys is a promising approach for weight reduction and improved performance of such systems through improvement in design optimization with complex geometric components or by the substitution of material in components that are currently produced from titanium or ferrous alloys. However, there are two significant barriers to successful adoption of AM Al alloys. First, many critical applications require high-temperature (>200°C) strength retention, and most conventional age-hardened Al alloys lose much of their strength at elevated temperatures as strengthening precipitates coarsen and dissolve. Second, even given these limitations, the most desirable conventional Al alloys suffer from hot tearing in casting, welding, and additive manufacturing [1], significantly limiting the available alloy selection space to only compositions with less attractive property sets. Due to this lack of alloy selection for light-weight components, several new classes of Al alloys are in early stages of development and commercialization for AM, including Al-Zr-Mg [2,3], Al-Sc alloys [4–7], and modified wrought compositions that use nano-scale grain refiner particles to alleviate hot tearing [8].

In a recent review article [9], ORNL researchers outlined the general approaches to designing new AM capable Al alloys for elevated temperature applications. Among these, alloys with high fractions of intermetallics (HiFI alloys) are very promising. In such alloys, high cooling rates create a fine distribution of intermetallic particles upon solidification. Alloying additions with low diffusivity and solubility in Al may be selected to help increase coarsening resistance. This combination offers significant opportunities for strengthening that may retained even for very long service lives at elevated temperatures. In particular, Ce is an attractive alloying element, as it has a vanishingly small solubility in Al, a relatively low diffusivity, and also forms a eutectic reaction at approximately 10 wt.% Ce, which helps to eliminate hot-tearing during processing [10].

In response to these opportunities, ORNL has investigated a variety of Ce containing Al alloys for additive manufacturing. Al-Ce-Mg [11] showed excellent strength, but suffered from challenges in processing due to the high vapor pressure of Mg, leading to increased vaporization and propensity for keyhole formation and changes in alloy composition. Al-Ce-Mn alloys [12,13] exhibit stability in mechanical properties at high temperatures, but have low ductility due to extremely high intermetallic phase content. Al-Cu-Ce alloys [14–16] are very processable and have good strength, especially when Zr is added for additional strengthening through precipitation of Al_3Zr $L1_2$ nanoparticles. However, the Al-Ce-Ni family of alloys has shown the greatest promise, with exceptional room temperature and high-temperature strength, creep, and fatigue resistance [17,18]. The Al-Ce-Ni system exhibits a ternary eutectic reaction, which is desirable for processability. Small amounts of Mn may be added to offer some additional solid solution strengthening and to encourage solidification of more thermally stable intermetallic variants [19]. Zr may also be added as a grain refiner and to promote $L1_2$ nanoparticles upon heat treatment.

A particular variant within the Al-Ce-Ni system, with nominal composition Al-9Ce-4Ni-0.5Mn-1Zr (wt.%), and dubbed DuAlumin-3D, has been developed by ORNL. The alloy shows excellent printability and initial testing indicates very high creep resistance, fatigue resistance, and thermal stability. The purpose of this collaboration with Boeing is to manufacture additional material of this particular alloy and to evaluate a key set of mechanical test conditions of relevance to aerospace applications.

1.2 TECHNICAL RESULTS

1.2.1 Additive Manufacturing and Heat Treatment

Ingots of DuAlumin-3D were alloyed by Eck Industries, and then were nitrogen gas atomized by Connecticut Engineering Associated Inc. After atomization, the composition of the powder was characterized using inductively coupled plasma. Table 1 shows a summary of the nominal and measured alloy composition. The Ce content was somewhat lower than expected, and the Ni content was slightly higher than nominal. The Zr content was lower than specified, Zr is notoriously hard to control precisely and some losses are generally anticipated. The value obtained here is similar to previous batches of material. The Si impurity content was within specifications. The Fe impurity was slightly above specification, but recent research has demonstrated that elevated Fe content in Al-Ce-Ni alloys is not necessarily detrimental [20].

Table 1: Nominal and measured powder composition.

	Al	**Ce**	**Ni**	**Mn**	**Zr**	**Si**	**Fe**
Nominal	Bal.	9	4	0.5	1	<0.1	<0.1
Measured	Bal.	7.53	4.72	0.5	0.65	0.054	0.12

Additive manufacturing was performed at Beehive Industries using an EOS M290 laser powder bed fusion (LPBF) system. The processing parameters used for manufacturing are summarized in Table 2. Coupons were manufactured for mechanical testing with axes either parallel or perpendicular to the build direction, herein denoted Z and XY respectively. Figure 1 shows a photograph of a characteristic build. Coupons were cut from the build plate and tested in the as-printed (AP) condition, or following an age-hardening heat treatment (T5) at 350 °C for 8 h.

Table 2: Summary of LPBF processing parameters.

Power (W)	**Velocity (mm/s)**	**Hatch Spacing (mm)**	**Layer Thickness (µm)**	**Preheat Temperature (°C)**
370	1300	0.19	30	150

Figure 1: Example of AM samples producing for machining mechanical test coupons.

After build plate removal and heat treatment, samples were machined and then mechanically tested. Tensile testing was performed at room temperature, 93, 204, 343, and 398 °C according to the ASTM E21 standard. Room temperature fatigue testing was also performed for each of the selected coupon directions and heat treatment conditions. Fatigue test was performed at 20 Hz with R = -1 for a range of stress levels.

1.2.2 Tensile Testing

Figure 2 shows a selection of representative room temperature tensile curves. Note that the discontinuity in the stress-strain curves is related to a change in strain rate applied following yielding in accordance with the ASTM E21 standard. First, the tensile results show that the room temperature yield strength and ultimate tensile strength of the alloy tend to increase following heat treatment as a result of the precipitation of Al_3Zr $L1_2$ nanoparticles. The alloy also tends to exhibit higher strength in the XY plane compared to along the build direction in both the as-printed and heat treated conditions.

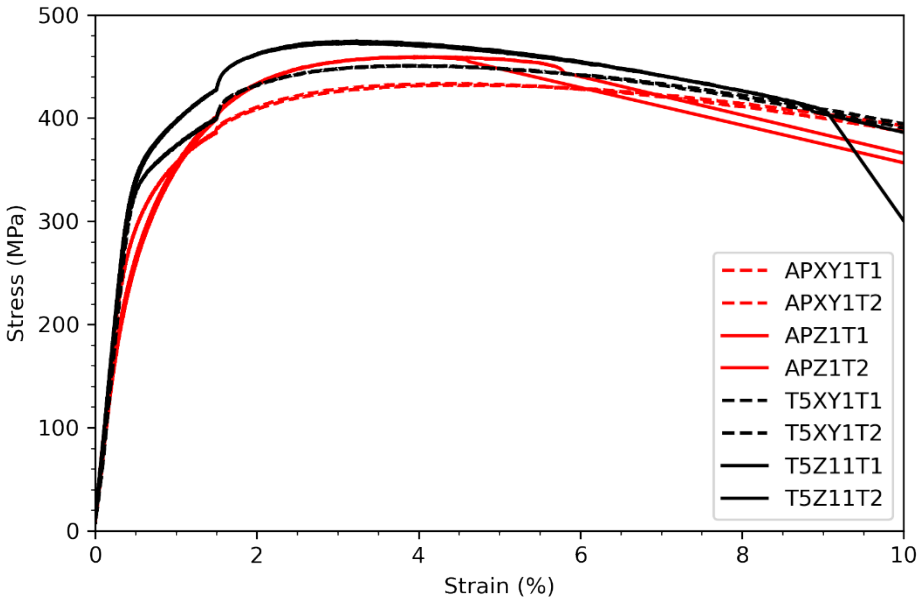

Figure 2: Representative tensile curves for AM samples in as-fabricated and heat treated conditions, and in the build direction, or within the build plane.

The tensile properties of the alloy were also compared as a function of temperature. Figure 3 shows a comparison of the as-printed condition results for yield strength and ultimate tensile strength, and with respect to the test direction, as a function of temperature. As expected, the yield and ultimate tensile strength tend to decrease with temperature. The XY direction is slightly stronger from room temperature up until about 200 °C, but the difference in strength reduces at higher temperatures. Additionally, a significant amount strain hardening is present at room temperature, as indicated by the difference in yield and ultimate tensile stresses, but the amount of hardening decreases significantly at higher temperatures. Overall, the strength of the alloy is reasonable compared with conventional cast and wrought Al alloys at room temperature. However, the strength retention at elevated temperature is exceptional, where most conventional precipitation hardenable alloys lose the vast majority of their strength above about 200 °C.

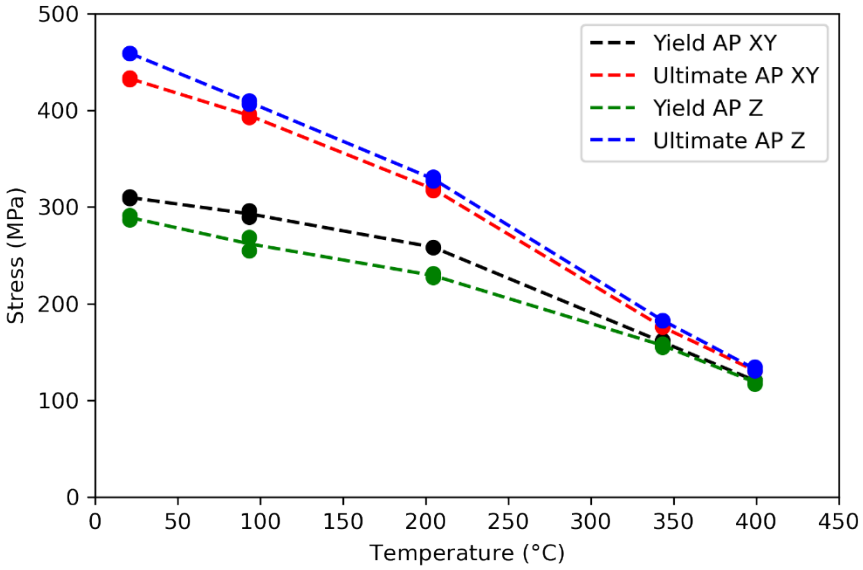

Figure 3: Comparison of XY and Z direction tests as a function of temperature for as-printed specimens.

Figure 4 shows a summary graph of the tensile properties for the heat treated (T5) condition for the alloy as a function of temperature. Overall, a similar trend is found as the as-printed samples, in that the yield and ultimate tensile strength decreases with temperature, as does the total amount of strain hardening. Interestingly, however, the anisotropy found in the yield strength of the as-printed samples has decreased following heat treatment, and the strength is similar in both the XY and Z directions, with perhaps only a small difference found at room temperature.

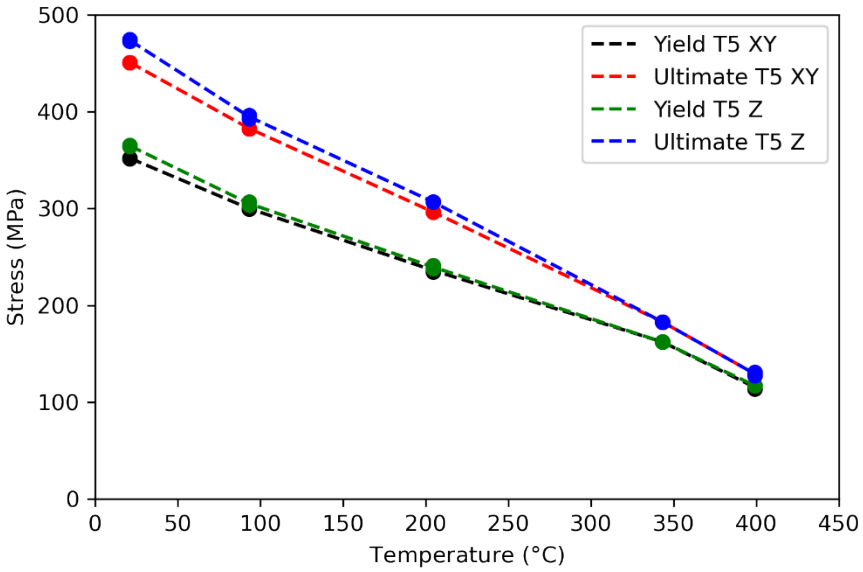

Figure 4: Comparison of XY and Z direction tests as a function of temperature for aged specimens.

Figure 5 shows a direct comparison of the as-printed and heat treated tensile results as a function of temperature. The XY direction was selected as representative in this case. The heat treated sample shows higher yield and ultimate tensile strengths at room temperature. However, the difference between these conditions is smaller for higher temperatures, becoming negligible between approximately 350 and 400 ° C.

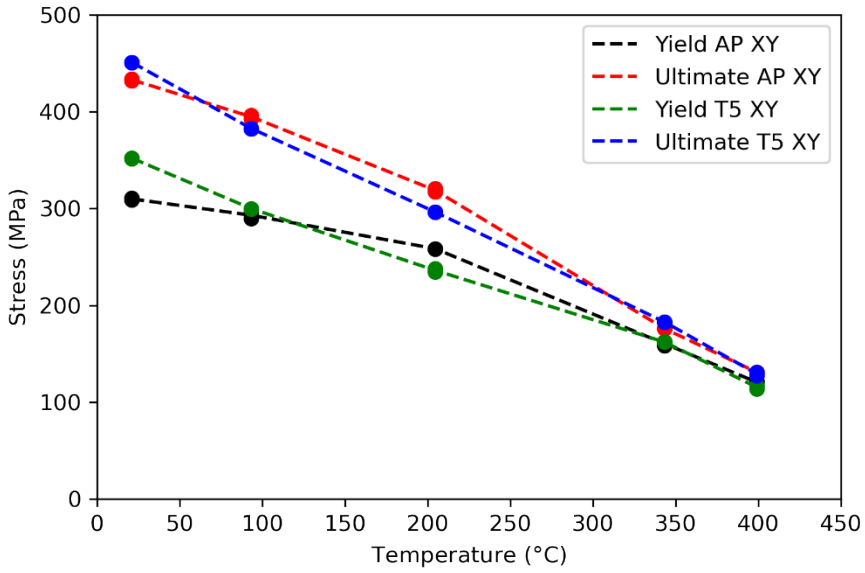

Figure 5: Comparison of as-printed and heat treated specimens as a function of temperature in the XY plane.

Figure 6 shows a comparison of the total elongation at fracture for each of the conditions as a function of temperature. First, the elongation of the alloy in both as-printed and heat treated conditions is reasonable at room temperature, ranging from 5 to 11%. However, the as-fabricated alloy does show a lower total elongation at room temperature along the Z direction. Some of this ductility is recovered following heat treatment, but is still lower than the XY samples, for which the total elongation is similar in both the as-fabricated and heat treated conditions. The total elongation tends to increase with temperature in all cases up to about 100°C. However, for intermediate temperature between 100 and 350 ° C, the results diverge. In the XY direction, the alloy continues to gain ductility as expected up to 200°C. However, the Z direction samples show a significant ductility dip in this range, with a lower elongation at 200 °C than at 100 °C. This result is consistent with previous reports of an intermediate temperature ductility dip in additively manufactured Al-Cu-Ce based alloys for a similar temperature range [14] which was found to be associated with variations in strain rate sensitivity related to microstructural heterogeneities near melt pool boundaries. At 350°C, the alloy regains ductility along the Z direction, but loses ductility in the XY direction. At 400°C, all condition converge, showing a relatively similar elongation in all cases, though it is lower than would be expected for conventional alloys at similar temperatures.

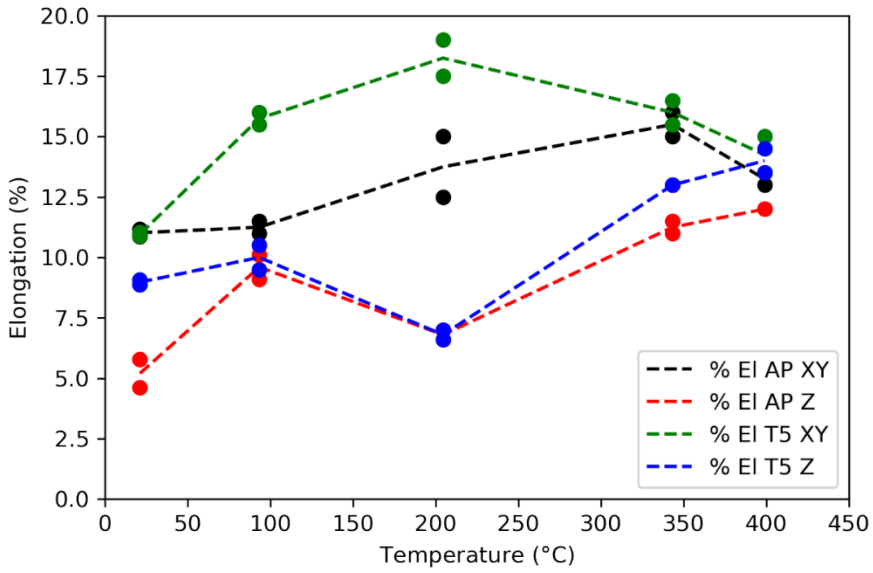

Figure 6: Elongation at fraction for as-printed and T5 conditions as a function of temperature, compared for both XY and Z samples.

1.2.3 Fatigue Testing

High cycle fatigue testing was conducted at room temperature for a range of stress levels, for each orientation, and in the as-printed (AP) and heat treated (T5) conditions. The results of the fatigue testing are shown in Figure 7. In the as-printed state, a significant anisotropy was observed between the XY and Z direction samples, with samples oriented perpendicular to the build direction showing much higher overall fatigue resistance. Note that three tests reached the maximum number of cycles for this study (2x 10^6) and the tests were stopped without failure. Interestingly, following heat treatment, the anisotropy decreases significantly. Overall, the fatigue resistance of the horizontal (XY) samples does not changes dramatically with heat treatment, but the fatigue resistance of the vertical (Z) samples increase substantially. It is possible that fatigue failure for the vertical samples is associated with local variations in the microstructure at melt pool boundaries, as has been identified for tensile and creep properties in a variety of AM Al alloys [14,17]. The change in fatigue strength for the vertical specimens with heat treatment may then be correlated with a microstructural change in the melt pool boundaries during heat treatment. Additional characterization and research will be necessary to establish these links between processing, microstructure, and the fatigue properties.

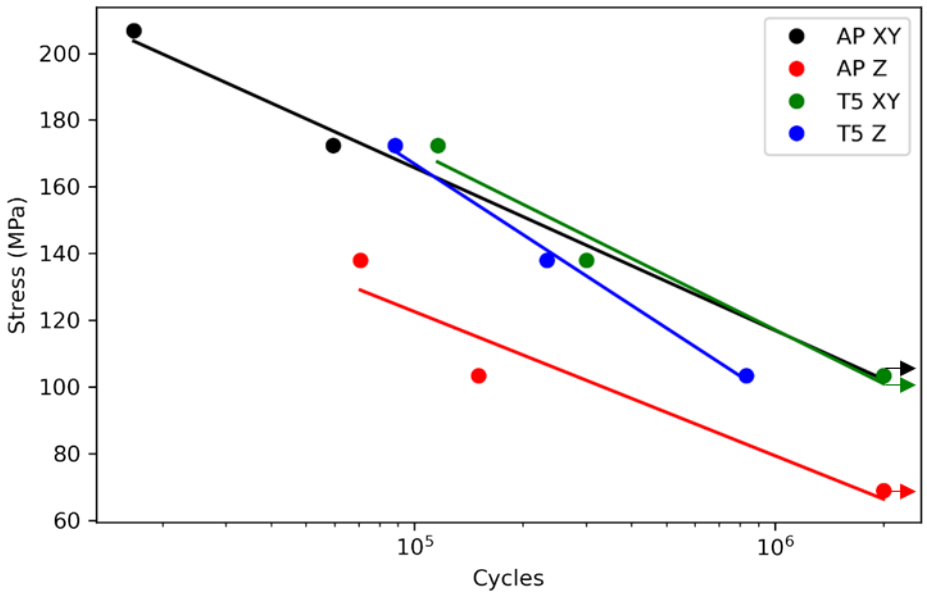

Figure 7: Comparison of room temperature high cycle fatigue results.

1.2.4 COMPARISON TO 2219

The mechanical properties results were compared against 2219-T61 as a representative wrought Al alloy widely used in the aerospace industry. Figure 8 shows a directly comparison of the tensile properties for both alloys as a function of temperature. DuAlumin-3D has a higher yield and ultimate strength at room temperature, and importantly, maintains a much higher fraction of this strength at temperature up to 400° C, whereas 2219 loses more than 90% of its strength over the same temperature range. This trend is expected as 2219 is primarily strengthened by precipitates that form during the aging process, and this strength is lost as those precipitates coarsen and dissolve during testing at elevated temperatures. Both alloys have similar elongation between room temperature and approximately 200°C. However, as 2219 softens at higher temperatures, the elongation increases dramatically, while DuAlumin-3D retains an elongation between about 10 and 20%.

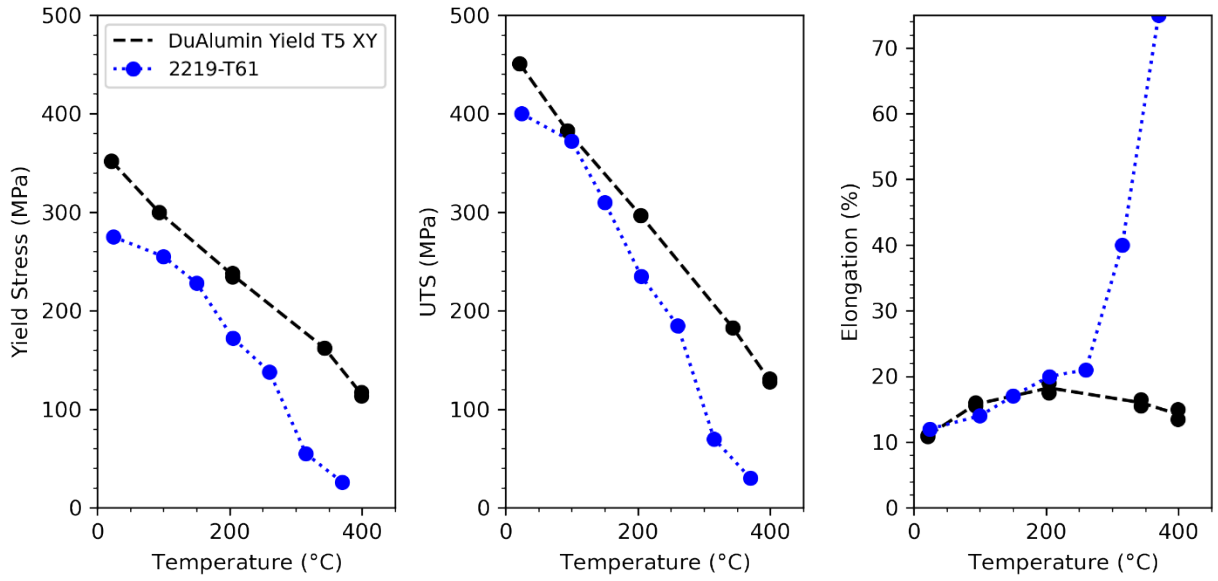

Figure 8: Comparison of tensile properties between DuAlumin-3D and wrought 2618-T61.

According to handbook values, 2219 has a room temperature fatigue strength (measured at $5x10^8$ cycles) of 105 MPa. For a similar stress level, runout of $2x10^6$ cycles was achieved for horizontal (XY) samples in both the as-printed and heat treated conditions. It may be concluded from this data that the alloy may meet, but not exceed, the room temperature high-cycle fatigue performance of 2219. Additional research will be necessary to identify the failure mode of DuAlumin-3D and determine if increases in fatigue life are possible. For example, previous research on a related alloy has identified Ce-rich oxide inclusions as a source of fatigue crack initiation [18]. Additionally, the most important performance metrics for DuAlumin-3D are for elevated temperature applications. Given the very high tensile strength in the high-temperature regime compared to 2219, it is possible that fatigue performance in for these conditions will meet or exceed those of common wrought alloys.

1.4 CONCLUSIONS

In this study, DuAlumin-3D, an ORNL designed alloy with nominal composition Al-9Ce-4Ni-0.5Mn-1Zr (wt.%) was fabricated using additive manufacturing. Samples were produced in both vertical and horizontal directions relative to the AM build direction. These samples were machined for tensile and fatigue testing, and tested in either the as-printed state, or following a T5 direct-age heat treatment of 8 h at 350°C. The tensile properties as a function of temperature were found to be somewhat anisotropic in the as-printed state, but the anisotropy diminished after heat treatment. The elongation also showed an intermediate temperature ductility dip. Overall, the tensile performance was excellent across all temperatures as compared to a baseline 2219-T61 alloy. Room temperature fatigue test exhibited significant anisotropy in the as-fabricated case, which was almost entirely removed with heat treatment. The alloy compared exhibited a room temperature fatigue resistance that we similar to, but not better than 2219-T61. Additional testing and characterization is recommended to identify the microstructure features associated with the anisotropy in tensile properties and the failure mode in fatigue.

1.5 REFERENCES

[1] S. Kou, A criterion for cracking during solidification, Acta Mater. 88 (2015) 366–374. https://doi.org/10.1016/j.actamat.2015.01.034.

[2] J.R. Croteau, S. Griffiths, M.D. Rossell, C. Leinenbach, C. Kenel, V. Jansen, D.N. Seidman, D.C. Dunand, N.Q. Vo, Microstructure and mechanical properties of Al-Mg-Zr alloys processed by selective laser melting, Acta Mater. 153 (2018) 35–44. https://doi.org/10.1016/j.actamat.2018.04.053.

[3] S. Griffiths, M.D. Rossell, J. Croteau, N.Q. Vo, D.C. Dunand, C. Leinenbach, Effect of laser rescanning on the grain microstructure of a selective laser melted Al-Mg-Zr alloy, Mater. Charact. (2018).

[4] A.B. Spierings, K. Dawson, P.J. Uggowitzer, K. Wegener, Influence of SLM scan-speed on microstructure, precipitation of Al3Sc particles and mechanical properties in Sc- and Zr-modified Al-Mg alloys, Mater. Des. (2017). https://doi.org/10.1016/j.matdes.2017.11.053.

[5] R. Li, M. Wang, T. Yuan, B. Song, C. Chen, K. Zhou, P. Cao, Selective laser melting of a novel Sc and Zr modified Al-6.2 Mg alloy: Processing, microstructure, and properties, Powder Technol. 319 (2017) 117–128. https://doi.org/10.1016/j.powtec.2017.06.050.

[6] Material Data Sheet - Scalmalloy, Taufkirchen, Germany, n.d.

[7] M. Awd, J. Tenkamp, M. Hirtler, S. Siddique, M. Bambach, F. Walther, Comparison of Microstructure and Mechanical Properties of Scalmalloy® Produced by Selective Laser Melting and Laser Metal Deposition, Materials. 11 (2017) 17. https://doi.org/10.3390/ma11010017.

[8] J.H. Martin, B.D. Yahata, J.M. Hundley, J.A. Mayer, T.A. Schaedler, T.M. Pollock, 3D printing of high-strength aluminium alloys, Nature. 549 (2017) 365–369. https://doi.org/10.1038/nature23894.

[9] R.A. Michi, A. Plotkowski, A. Shyam, R.R. Dehoff, S.S. Babu, Towards high-temperature applications of aluminium alloys enabled by additive manufacturing, Int. Mater. Rev. 67 (2022) 298–345. https://doi.org/10.1080/09506608.2021.1951580.

[10] F. Czerwinski, Cerium in aluminum alloys, J. Mater. Sci. 55 (2020) 24–72. https://doi.org/10.1007/s10853-019-03892-z.

[11] K. Sisco, A. Plotkowski, Y. Yang, D. Leonard, B. Stump, P. Nandwana, R.R. Dehoff, S.S. Babu, Microstructure and Properties of Additively Manufactured Al-Ce-Mg Alloys, (n.d.) 20.

[12] K.D. Sisco, A. Plotkowski, Y. Yang, L. Allard, C. Fancher, C. Rawn, J.D. Poplawsky, R. Dehoff, S.S. Babu, Heterogeneous phase transformation pathways in additively manufactured Al-Ce-Mn alloys, J. Alloys Compd. 938 (2023) 168490. https://doi.org/10.1016/j.jallcom.2022.168490.

[13] A. Plotkowski, K. Sisco, S. Bahl, A. Shyam, Y. Yang, L. Allard, P. Nandwana, A.M. Rossy, R.R. Dehoff, Microstructure and properties of a high temperature Al–Ce–Mn alloy produced by additive manufacturing, Acta Mater. 196 (2020) 595–608. https://doi.org/10.1016/j.actamat.2020.07.014.

[14] S. Bahl, A. Plotkowski, K. Sisco, D.N. Leonard, L.F. Allard, R.A. Michi, J.D. Poplawsky, R. Dehoff, A. Shyam, Elevated temperature ductility dip in an additively manufactured Al-Cu-Ce alloy, Acta Mater. 220 (2021) 117285. https://doi.org/10.1016/j.actamat.2021.117285.

[15] S. Bahl, K. Sisco, Y. Yang, F. Theska, S. Primig, L.F. Allard, R.A. Michi, C. Fancher, B. Stump, R. Dehoff, A. Shyam, A. Plotkowski, Al-Cu-Ce(-Zr) alloys with an exceptional combination of additive processability and mechanical properties, Addit. Manuf. 48 (2021) 102404. https://doi.org/10.1016/j.addma.2021.102404.

[16] S. Bahl, A. Plotkowski, T.R. Watkins, R.A. Michi, B. Stump, D.N. Leonard, J.D. Poplawsky, R. Dehoff, A. Shyam, 3D printed eutectic aluminum alloy has facility for site-specific properties, Addit. Manuf. 70 (2023) 103551. https://doi.org/10.1016/j.addma.2023.103551.

[17] R.A. Michi, K. Sisco, S. Bahl, Y. Yang, J.D. Poplawsky, L.F. Allard, R.R. Dehoff, A. Plotkowski, A. Shyam, A creep-resistant additively manufactured Al-Ce-Ni-Mn alloy, Acta Mater. 227 (2022) 117699. https://doi.org/10.1016/j.actamat.2022.117699.

[18] R.A. Michi, J.J. Simpson, S. Bahl, Q. Campbell, P. Brackman, A. Plotkowski, R.R. Dehoff, J.A. Haynes, Q. Wang, A. Shyam, Additively manufactured Al-Ce-Ni-Mn alloy with improved elevated-

temperature fatigue resistance, Addit. Manuf. 66 (2023) 103477. https://doi.org/10.1016/j.addma.2023.103477.
[19] A.E. Perrin, R.A. Michi, D.N. Leonard, K.D. Sisco, A.J. Plotkowski, A. Shyam, J.D. Poplawsky, L.F. Allard, Y. Yang, Effect of Mn on eutectic phase equilibria in Al-rich Al-Ce-Ni alloys, J. Alloys Compd. 965 (2023) 171455. https://doi.org/10.1016/j.jallcom.2023.171455.
[20] T. Wu, A. Plotkowski, A. Shyam, D.C. Dunand, Microstructure and mechanical properties of hypoeutectic Al–6Ce–3Ni-0.7Fe (wt.%) alloy, Mater. Sci. Eng. A. 875 (2023) 145072. https://doi.org/10.1016/j.msea.2023.145072.

2. BOEING BACKGROUND

Boeing is the world's largest aerospace company and leading manufacturer of commercial jetliners, defense, space and security systems, and service provider of aftermarket support. As America’s biggest manufacturing exporter, the company supports airlines and U.S. and allied government customers in more than 150 countries. Boeing products and tailored services include commercial and military aircraft, satellites, weapons, electronic and defense systems, launch systems, advanced information and communication systems, and performance-based logistics and training.